Probing the strong electroweak symmetry breaking in a model with a vector resonance

M. Gintner[1,2], **I. Melo**[1], **B. Trpišová**[1]

[1] *Physics Department, University of Žilina, Žilina*
[2] *Science and Research Institute, Matej Bel University, Banská Bystrica*

I Introduction

Despite the great success of the Standard model of electroweak interactions (SM) one essential component of the theory remains a puzzle. It is well known that to maintain the gauge invariance principle at work a spontaneous breaking of the electroweak symmetry has to take place in the SM. However, the actual mechanism behind the electroweak symmetry breaking (ESB) remains unknown. The Higgs complex doublet scalar field of a non-zero vacuum expectation value serves as a benchmark hypothesis for the mechanism. A direct consequence of the hypothesis is the presence of the Higgs boson in the particle spectrum of the SM, not observed to these days though.

The LHC is a supreme machine to search for the Higgs boson. However, the introduction of the Higgs field is not the only possibility how to break the electroweak symmetry. In addition, there are serious theoretical objections to this scenario. Therefore, it makes sense to investigate the potential of the LHC to distinguish signs of alternative ESB mechanisms.

The minimal scenario of ESB requires a triplet of scalar fields to provide three extra degrees of freedom of electroweak gauge bosons once they receive their masses. It implies no additions to the SM particle spectrum, neither the Higgs boson nor any other new particle. In this case the ESB sector of the SM would have a form of the non-renormalizable non-linear sigma model. While such an arrangement can accommodate all nowadays experimental measurements and observations it violates tree-level unitarity at the energy scale of about 1 TeV. Thus its validity would be limited and it would require an onset of new physics at or below this scale. Thus it seems reasonable to complement this minimal non-linear sigma model scenario with a new non-SM field(s) which would restore unitarity of the theory. In the case of the SM Higgs boson the unitarity restoration is the most obvious theoretical reason why we expect its mass to be below 1 TeV.

There is a host of candidates for the suitable extensions of the SM. They range from supersymmetric theories with multiple elementary Higgs bosons in their spectra to the theories of new strong interactions, like in Technicolor, which might form bound states of new elementary particles in analogy with QCD. These bound states might appear in the particle spectrum as new resonances. One of their roles would be to unitarize scattering amplitudes. In more recent theories like the Little Higgs models and the Gauge-Higgs unification models, their dual-description relation to the Heavy Composite Higgs and the No Higgs strongly-interacting models has been demonstrated (see [1] and references therein). Most of these new models introduce new quarks and new vector particles at about 1 TeV.

Facing this plethora of alternative theories it is highly desirable to describe their low-energy phenomenology in a unified way. Thus, it is very useful to exploit the formalism of effective Lagrangians. In this approach the non-linear sigma model would represent the lowest-order term of the effective Lagrangian. As noted above it is reasonable to expect the existence of a new field unitarizing tree-level amplitudes at 1 TeV. Once the transformation properties of the field are chosen it can be introduced in the effective Lagrangian in quite a straightforward manner bringing in new free parameters which have to be obtained from experiment.

There is also a more involved procedure in introducing a new vector field(s) in the non-linear effective Lagrangian. This procedure uses the so-called *hidden local symmetry* (HLS) approach [2]. Any non-linear sigma model based on the coset space G/H is gauge equivalent to a linear model possessing $G_{global} \times H_{local}$ symmetry. To gauge the H-component of the symmetry vector gauge-boson fields $V_\mu^a(x)$, $a = 1, \ldots, \dim H$, have to be introduced. There is a gauge in which this "linear" model takes on the form of the G/H non-linear sigma model. If also fermions and the gauge-bosons of a subgroup of G are introduced in the HLS model, then, after fixing the hidden gauge, we end up with the non-linear Callan-Coleman-Wess-Zumino Lagrangian [3, 4]. The HLS formalism along with the AdS/CFT correspondence plus deconstruction is behind the dual-description relation of the recent models mentioned above [1].

Following the HLS approach in the case of the ESB sector the G group is $SU(2)_L \times SU(2)_R$, while $H = SU(2)_V$. Along with the SM fermions and the $SU(2)_L \times U(1)_Y$ gauge bosons the $SU(2)_V$ gauge-boson triplet is present. After fixing the proper gauge for the $SU(2)_V$ symmetry the HLS model turns to the non-linear model of the ESB sector with the extra triplet of vector bosons. An effective Lagrangian built this way contains less free parameters because some of them are related. For example, the masses of the $SU(2)_V$ gauge-boson triplet depend on the coupling constants. In addition, $SU(2)_V$ gauge bosons mix with the electroweak gauge bosons. This approach was applied in formulating the so-called BESS (Breaking Electroweak Symmetry Strongly) model (e.g. [5] and references therein) which pioneered the use of the HLS approach to the effective description of new resonances formed by new strong interactions related to the ESB.

While the mixing complicates theoretical analysis of the model it might provide some advantages in experimental searches. It is natural to assume that apart from the electroweak gauge bosons the new vector triplet couples to the third generation of quarks only. This is motivated by the extraordinary mass of the top quark when compared to other SM fermions: it is very high and close to the ESB scale. Thus the top quark, and possibly b quark too, might be involved in physics responsible for the ESB. It might manifest itself through their direct coupling to the new vector resonances. Therefore it would seem natural to search for the signs of the resonances in the processes where besides the electroweak bosons the t and b quarks are involved. At the LHC this is often a difficult case due to the large backgrounds to the processes with b and t in the final state and/or due to the negligible b and t luminosities in pp collisions. However, the mixing of the vector resonances with the electroweak gauge bosons generates interactions of the new resonances to the fermions of lighter generations. Although these interactions are suppressed by the mixing factors, the processes enabled by them have the advantage of higher parton luminosities and more favorable final state topologies, on the other hand.

In this paper we would like to report on our investigation of the LHC two-particle finel state processes which might be sensitive to the couplings of the new vector resonances in the HLS based Higgsless models with a single new $SU(2)_V$ vector triplet. In the next Section we briefly introduce

our effective Lagrangian. In Section III we present results of our analysis. In Conclusions we summarize our findings and outline the prospective steps of this investigation.

II Lagrangian

The overall Lagrangian of the modified BESS model [6] with the $SU(2)_V$ vector triplet field $\{\rho_\mu^a\}_{a=1}^3$ is

$$L = \frac{v^2}{4}\mathrm{Tr}(D_\mu U^\dagger D^\mu U) - a\frac{v^2}{4}\mathrm{Tr}(\mathcal{V}_\mu \mathcal{V}^\mu) + L^f + L_{kin}(W) + L_{kin}(B) + L_{kin}(\rho), \tag{1}$$

where L_{kin}'s denote the kinetic terms of the gauge fields. They also induce self-interactions in the case of the non-abelian fields W and ρ. The first term in (1) is the gauged non-linear sigma model of the scalar triplet $\{\pi_a(x)\}_{a=1}^3$ with $U(x) = \exp(2i\vec{\pi}\vec{\tau}/v)$, where $\tau_a = \sigma_a/2$ $(a = 1, 2, 3)$ stands for the $SU(2)$ group generators, σ_a being the Pauli matrices, and $v \approx 246$ GeV. The covariant derivative reads

$$D_\mu U = \partial_\mu U - iU\mathcal{L}_\mu + i\mathcal{R}_\mu U, \quad \mathcal{L}_\mu \equiv g\vec{W}_\mu\vec{\tau}. \quad \mathcal{R}_\mu \equiv g' B_\mu \tau_3$$

Here, $\vec{W}_\mu$ denotes the $\mathrm{SU}(2)_L$ gauge boson triplet, and B_μ is the $\mathrm{U}(1)_Y$ gauge boson.

The first two terms in (1) are responsible for the masses of the gauge bosons and their mutual mixing. There,

$$\mathcal{V}_\mu = \frac{1}{2}(\xi^\dagger\partial_\mu\xi + \xi\partial_\mu\xi^\dagger) + ig_V\vec{\rho}_\mu\vec{\tau} + \frac{i}{2}(\xi\mathcal{L}_\mu\xi^\dagger + \xi^\dagger\mathcal{R}_\mu\xi), \quad \xi(x) = \exp(i\vec{\pi}(x)\vec{\tau}/v).$$

In the limit of large g_V the masses of the charged gauge field mass eigenstates are

$$M_{\rho^\pm} = \frac{\sqrt{a}vg_V}{2}\left[1 + \frac{1}{4}\left(\frac{g}{g_V}\right)^2 + \frac{1}{4a}\left(\frac{g}{g_V}\right)^4\right]^{1/2}, \quad M_{W^\pm} = \frac{vg}{2}\left[1 - \frac{1}{4}\left(\frac{g}{g_V}\right)^2\right]^{1/2},$$

and the masses of the neutral mass eigenstates are

$$M_{\rho^0} = \frac{\sqrt{a}vg_V}{2}\left[1 + \frac{1}{4}\left(\frac{G}{g_V}\right)^2 + \frac{(g^2 - g'^2)^2}{4ag_V^4}\right]^{1/2}, \; M_Z = \frac{vG}{2}\left[1 - \frac{(g^2 - g'^2)^2}{4G^2g_V^2}\right]^{1/2},$$

where $G = \sqrt{g^2 + g'^2}$. The mass of photon is zero, of course.

The term L^f is responsible for the interactions of fermions to the gauge bosons including the vector ρ-resonances

$$L^f = L^f_{SM} + L_\rho^{(t,b)_L} + L_\rho^{(t,b)_R} - (\bar{\psi}_L^j U^\dagger M_j \psi_R^j + \mathrm{h.c.}) \tag{2}$$

where L^f_{SM} is the part of the fermion Lagrangian which, besides fermion kinetic terms, contains the SM interactions of fermions to the electroweak gauge bosons. Further, $\{\psi^j\}_{j=1}^6$ are usual doublets of the SM fermions, and $M_j = \mathrm{diag}(m_j^u, m_j^d)$ are the fermion doublet mass matrices.

The core of new physics interactions of fermions lies in the second and third terms of (2). The BESS model considered in the literature possesses the ρ-to-fermion coupling inter-generation universality [5] which leads to stringent limits on these couplings from the existing measurements of the SM parameters. In an attempt to reflect the speculations about a special role of the top quark (or the third quark generation) in the mechanism of ESB we modify the fermion sector by considering no direct interactions of ρ to the fermions other than t and b. In addition, the $SU(2)_L$ symmetry does not allow us to disentangle the ρ-to-t_L coupling from the ρ-to-b_L one. However, it can be done in the case of right fermions. We do it and to simplify the numerical analysis of the model we turn off completely the direct interaction of ρ to b_R. Then

$$L_\rho^{(t,b)_L} = \frac{b_1}{1+b_1} g\ \bar{\psi}_L \not{W}_a \tau_a \psi_L + \frac{b_1}{1+b_1} g_V\ \bar{\psi}_L \not{\rho}_a \tau_a \psi_L \quad (3)$$

$$L_\rho^{(t,b)_R} = \frac{b_2}{1+b_2} g'(\bar{\psi}_R P_0)\ \not{B} \tau_3 (P_0 \psi_R) + \frac{b_2}{1+b_2} g_V (\bar{\psi}_R P_0)\ \not{\rho}_3 \tau_3 (P_0 \psi_R) \quad (4)$$

where $\psi = (t,b)^T$, and $P_0 = \mathrm{diag}(1,0)$. As a consequence of turning off the ρ-to-b_R coupling neither t_R directly couples to the charged ρ-resonance, as can be seen in (4).

The measurement of $Zb\bar{b}$ vertex constrains the ρ-to-t_L coupling to relatively small values. However, when the disentangling is applied the measurement does not limit the ρ-to-t_R interaction. For the low-energy limits on the model parameters, see [6].

The symmetries of the model enable to introduce additional terms into the fermion Lagrangian (2), parameterized by two free parameters λ_1 and λ_2. When the ρ-to-b_R coupling is zero the λ-terms modify existing couplings but do not introduce any new interactions. The presence of the λ-terms can further relax the low-energy limits on the ρ-resonance couplings. Nevertheless, in our calculations we put $\lambda_1 = \lambda_2 = 0$.

III Two-particle final state processes

We test the model when the mass of the neutral ρ-resonance is $M_{\rho^0} = 1$ TeV. Depending on the model parameters ρ^0 decays predominantly through one or more of the following three channels: $t\bar{t}$, $b\bar{b}$, W^+W^-. When its mass is fixed the total width of ρ^0, as well as its branching ratios, depend on g_V, b_1, and b_2. The situation in the $g_V - b_1 - b_2$ parametric space is depicted in Figure 1. Note that due to the turning off of the ρ-to-b_R coupling there is no such a choice of parameters when the decay of ρ^0 to $b\bar{b}$ solely or to $b\bar{b}$ and W^+W^- dominates.

The parameters M_{ρ^0}, g_V, b_1, and b_2 also determine the mass of $\rho^\pm$ and its decay width and branching ratios. The $\rho^\pm$-resonance dominantly decays to $t\bar{b}/\bar{t}b$ and/or $W^\pm Z$. In Table 1 we show the points of the $g_V - b_1 - b_2$ parametric space we test in our calculations.

We implemented the Lagrangian (1) into the CompHEP software [8, 7] as one of its models. Numerical analysis was performed for several processes in the selected points of the parametric space. All calculations are at tree level.

III.1 Analysis

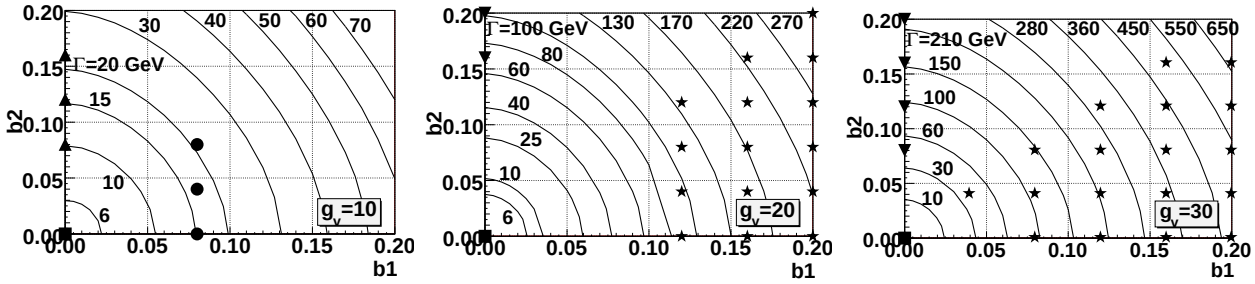

Figure 1: The total widths of ρ^0 depicted in the $g_V - b_1 - b_2$ parametric space. The markers distinguish areas of a clear domination of some channels; circles: $t\bar{t} \sim b\bar{b} \sim W^+W^-$, squares: $W^+W^- \gg t\bar{t}, b\bar{b}$, down-pointing triangles: $t\bar{t} \gg b\bar{b}, W^+W^-$, stars: $t\bar{t}, b\bar{b} \gg W^+W^-$, up-pointing triangles: $t\bar{t}, W^+W^- \gg b\bar{b}$.

P	g_V	b_1	b_2	Γ_{ρ^0}	BR(ρ^0)			$M_{\rho^\pm}$	$\Gamma_{\rho^\pm}$	BR($\rho^\pm$)	
				(GeV)	W^+W^-	$t\bar{t}$	$b\bar{b}$	(GeV)	(GeV)	$t\bar{b}/\bar{t}b$	$W^\pm Z$
1	10	0.08	0.04	16.899	31%	38%	31%	999.84	15.281	64%	36%
2	10	0.12	0.04	28.256	19%	42%	39%	999.84	26.433	79%	21%
3	10	0	0	5.334	99%	0.12%	0.08%	999.84	5.443	0.2%	98%
4	20	0	0.12	42.788	3%	97%	0.0025%	999.96	1.358	0.2%	98%
5	20	0.08	0	42.471	3%	46%	51%	999.96	42.509	97%	3%
6	35	0.04	0	34.580	1%	47%	52%	999.99	34.594	99%	1%
7	10	0	0.08	10.169	52%	48%	0.042%	999.84	5.443	0.18%	98%

Table 1: Properties of the ρ-triplet in the selected points of the $g_V - b_1 - b_2$ parametric space when $M_{\rho^0} = 1$ TeV.

We begin with the analysis of two-particle processes not only because they are the simplest ones to calculate but also to demonstrate that the visible ρ-resonance peaks can appear even in the presence of the mixing-suppressed couplings. There have been five such processes analyzed. They are listed in Table 2. The cuts have been introduced to maintain numerical stability of the calculations or to simulate the blind angle of the detector. No attempt to improve the signal-to-background ratio using cuts has been made.

We have considered six subprocesses contributing to $pp \to t\bar{t}X$ as well as to $pp \to b\bar{b}X$: $q\bar{q} \to t\bar{t}/b\bar{b}$, where $q = u, d, c, s, b$, and $gg \to t\bar{t}/b\bar{b}$. While the first four subprocesses of $\boldsymbol{pp \to t\bar{t}X}$ contain only ρ^0, $b\bar{b} \to t\bar{t}$ runs also through $\rho^\pm$ in t-channel. The gluon subprocess at tree level is not sensitive to new physics. There are visible ρ^0-peaks in the $m_{t\bar{t}}$-distribution of $b\bar{b} \to t\bar{t}$, when both, $\rho^0 \to t\bar{t}$ and $\rho^0 \to b\bar{b}$ channels, have a significant branching ratio (P=1,2,5,6). The peak disappears if one of the branching ratios gets small. The other $q\bar{q}$ subprocesses exhibit no noticeable peak structures in their $m_{t\bar{t}}$-distributions. In all the studied parametric space points the signal from $b\bar{b} \to t\bar{t}$ is overwhelmed by the $gg \to t\bar{t}$ background. No cuts have been applied though.

In the $\boldsymbol{pp \to b\bar{b}X}$ process only ρ^0 is present in all of the $q\bar{q}$ subprocesses. The cross sections for $q\bar{q} \to b\bar{b}$ do not depend on b_2. Again, the gluon subprocess at tree level is not sensitive to new physics. The region of the dominant $\rho^0 \to b\bar{b}$ decay should be the most favorable one for this

process	subprocess	P	ρ-peak visible	σ (pb)	cuts
$pp \to t\bar{t}X$	$gg \to t\bar{t}$	1–7	no	726	no
	$b\bar{b} \to t\bar{t}$	6	yes	1.69	
$pp \to b\bar{b}X$	$gg \to b\bar{b}$	1–7	no	1120	$m_{b\bar{b}} \geq 350$ GeV
	$b\bar{b} \to b\bar{b}$	5	yes	22.5	$-0.95 \leq c_{13}, c_{14} \leq 0.95$
$pp \to t\bar{b}X$	$u\bar{d} \to t\bar{b}$	2	yes	1.96	$-0.99 \leq c_{13}, c_{14} \leq 0.99$
	$c\bar{s} \to t\bar{b}$		yes	0.29	
	$u\bar{d} \to t\bar{b}$	5	yes	1.99	
	$c\bar{s} \to t\bar{b}$		yes	0.30	
	$u\bar{d} \to t\bar{b}$	SM	N/A	1.85	
	$c\bar{s} \to t\bar{b}$		N/A	0.28	
$pp \to W^+W^-X$	$u\bar{u} \to W^+W^-$	2	no	14.02	$-0.99 \leq c_{13}, c_{14} \leq 0.99$
	$b\bar{b} \to W^+W^-$		yes	0.77	
	$u\bar{u} \to W^+W^-$	3	yes	14.02	
	$b\bar{b} \to W^+W^-$		yes	0.74	
	$u\bar{u} \to W^+W^-$	SM	N/A	13.13	
	$b\bar{b} \to W^+W^-$		N/A	0.70	
$pp \to W^+ZX$	$u\bar{d} \to W^+Z$	1	yes	5.27	$-0.99 \leq c_{13}, c_{14} \leq 0.99$
	$c\bar{s} \to W^+Z$		yes	0.91	
	$u\bar{d} \to W^+Z$	3	yes	5.28	
	$c\bar{s} \to W^+Z$		yes	0.91	
	$u\bar{d} \to W^+Z^-$	SM	N/A	4.60	
	$c\bar{s} \to W^+Z^-$		N/A	0.79	

Table 2: Properties of the analyzed two-particle final state processes at $\sqrt{s} = 14$ TeV. Only the most important and interesting subprocesses and points P of the parametric space are displayed. The cross section values correspond to the $q\bar{q}' + \bar{q}'q$ initial states of the subprocesses. The SM results are calculated assuming $M_{Higgs} = 115$ GeV; c_{13} and c_{14} denote cosines of the scattering angles of the first and the second final state particles, respectively.

process. Indeed, out of P=1,2,5,6 the most visible peaks appear in the $m_{b\bar{b}}$- and the $p_T(b)/p_T(\bar{b})$-distributions of the $b\bar{b} \to b\bar{b}$ subprocess for $P = 5, 6$. The other $q\bar{q}$ subprocesses exhibit no noticeable peak structures in their distributions. However, this all is overwhelmed again by the contribution of the $gg \to b\bar{b}$ subprocess.

In the remaining three processes there are no gluon-gluon subprocesses. Only two subprocesses contribute to $\boldsymbol{pp \to t\bar{b}X}$: $u\bar{d} \to t\bar{b}$ and $c\bar{s} \to t\bar{b}$. There is also the charge conjugated process $pp \to \bar{t}bX$ which would increase the cross section usable for the charged ρ investigation. Feynman diagrams contain only the charged ρ-resonances and they are not sensitive to the value of b_2 except through the width of $\rho^{\pm}$. Considering P=2 and P=5, there are visible peaks in the $m_{t\bar{b}}$-distributions as well as in the $p_T(t)/p_T(\bar{b})$-distributions of the both subprocesses. Since these subprocesses are not overwhelmed by a contribution not sensitive to the model parameters it might be reasonable to consider also the use of the total cross section for the investigation of the model.

There are also two subprocesses contributing to $\boldsymbol{pp \to W^+ZX}$: $u\bar{d} \to W^+Z$ and $c\bar{s} \to W^+Z$. As in the previous case, there also is the charge conjugated process $pp \to W^-ZX$ which can be used to increase statistics. Feynman diagrams contain only the charged ρ-resonances. The amplitudes are sensitive to the values of b_1 and b_2 through the width of $\rho^\pm$ only. When we calculate at P=1 and P=3 the ρ-peaks are visible in the m_{WZ}-distributions as well as the $p_T(W)$- and $p_T(Z)$-distributions of the both subprocesses.

Five subprocesses contribute to $\boldsymbol{pp \to W^+W^-X}$: $q\bar{q} \to W^+W^-$, where $q = u, d, c, s, b$. Feynman diagrams contain only the neutral ρ-resonance. The amplitudes are not sensitive to b_2 except through the width of ρ^0. When P=1 or 2 there are visible peaks in the m_{WW}-distributions as well as the $p_T(W^+)$- and $p_T(W^-)$-distributions of the $b\bar{b}$ subprocess only. However, this subprocess has the smallest cross section of all the subprocesses. The dominant contribution comes from the $u\bar{u} \to W^+W^-$ and $d\bar{d} \to W^+W^-$ subprocesses, $\sigma(d\bar{d}) \approx 0.8\sigma(u\bar{u})$. When P=3 the peaks appear — not so pronounced though — in the distributions of all the subprocesses. The couplings of ρ^0 to b and t are comparable to the couplings of ρ^0 to the light quarks.

III.2 Results

Following the analysis performed in Subsection III.1 we calculate how well our model with various sets of parameters can be distinguished from the SM with the Higgs boson of the mass $M_{Higgs} = 115$ GeV. Since $pp \to t\bar{t}X$ and $pp \to b\bar{b}X$ are plagued by gluon-gluon backgrounds we focus on the remaining three processes in our calculations. No reducible backgrounds and no improving cuts are considered at this stage though.

In Figure 2 we show the final state pair of particles invariant mass distributions for the three studied processes. Therein, we have summed up contributions of all channels of a given process.

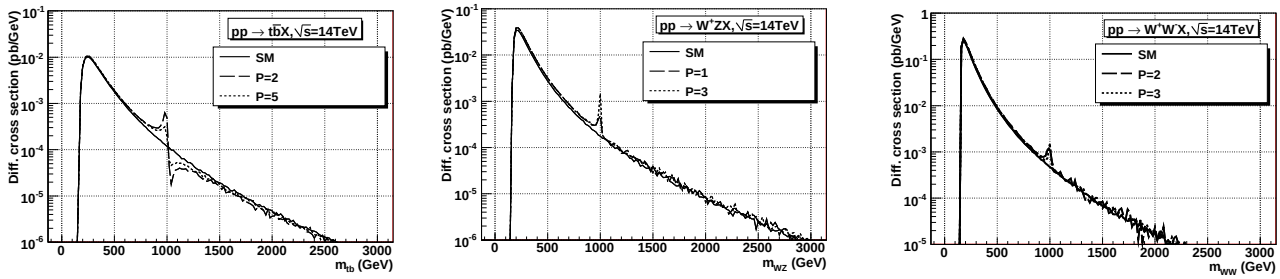

Figure 2: The final state pair of particles invariant mass distributions for the three studied processes. The curves are the sums of all the channels contributing to a given process. Various parametric space points have been considered. In each graph the solid line represents the SM.

We would like to know if the LHC signal by our model can be distinguished from the LHC signal of the SM. For that purpose we calculate the statistical significance of the model signal with respect to the SM

$$R = \frac{N_P - N_{SM}}{\sqrt{N_{SM}}}$$

process	P	cut	σ (pb)	R_0	R (100 fb^{-1})
$pp \to t\bar{b}X + c.c$	SM	no	5.84	0	0
	2		6.17	0.136	43.04
	SM	0.7 TeV $\leq m_{tb} \leq$ 1.1 TeV	0.14	0	0
	2		0.20	0.163	51.47
$pp \to W^+ZX + c.c$	SM	no	14.77	0	0
	3		16.96	0.570	180.37
	SM	0.7 TeV $\leq m_{WZ} \leq$ 1.1 TeV	0.20	0	0
	3		0.29	0.188	59.30
$pp \to W^+W^-X$	SM	no	29.86	0	0
	3		31.86	0.366	115.74
	SM	0.7 TeV $\leq m_{WW} \leq$ 1.1 TeV	0.37	0	0
	3		0.42	0.097	30.75

Table 3: Cross sections and statistical significance R of the model signals with respect to the SM for the studied processes when the integrated luminosity $\mathcal{L} = 100$ fb^{-1}. $R_0 = (\sigma_P - \sigma_{SM})/\sqrt{\sigma_{SM}}$.

where N_P and N_{SM} are the numbers of the events of our model and the SM, respectively. It is customary to consider as statistically significant such a deviation for which $R > 5$. We calculate R's based on the total cross sections as well as on the cross sections in the vicinity of the ρ peak, 0.7 TeV $\leq m_{34} \leq$ 1.1 TeV, where m_{34} is the final state pair of particles invariant mass. The obtained results are shown in Table 3.

Since none of the final state particles of the studied processes is stable, it is more relevant to consider the statistical significance when the decays are taken into account. In addition, also the question of detection efficiency of a given final state is important in evaluating more realistic values of R. In our calculations we consider the following reduction factors for the observed number of events: the efficiency of the b-jet detecting $\epsilon_b = 0.5$; the branching ratio $b^W_{jj} = \mathrm{BR}(W \to jj) = 0.64$, where j is a light-quark jet; $b^W_{\ell\nu} = \mathrm{BR}(W \to \ell\nu_\ell) = 0.11$, where ℓ is one of the charged SM leptons; $b^Z_{\ell\ell} = \mathrm{BR}(Z \to \ell^-\ell^+) = 0.034$; $b^Z_{jj} = \mathrm{BR}(Z \to jj) = 0.538$; $b^Z_{b\bar{b}} = \mathrm{BR}(Z \to b\bar{b}) = 0.153$. The obtained statistical significance for the processes after the final state decay is shown in Table 4.

We can see that the highest yields and statistical significance is in the channels that involve hadrons. At the same time though, these will be the channels with the richest and the most complicated backgrounds to deal with. The leptonic channels exhibit lesser event yield and lesser sensitivity. On the other hand, they provide cleaner signal and easily detectable particles, like muons. Thus, when selecting the most appropriate channels for probing our model it has to be a tradeoff between advantages and disadvantages of the both worlds. In addition, many of the channels displayed in Table 4 can be combined to reach higher statistics and/or complementary information on the properties of the model.

final state	reduction factor r	P	cut	events (100 fb^{-1})	R (100 fb^{-1})
$pp \to t\bar{b}X + c.c.$					
$\ell^+\nu_\ell b\bar{b} + c.c$	$\epsilon_b^2 b_{\ell\ell}^W$	2	no	1.70×10^4	7.14
	0.0275		yes	5.40×10^2	8.53
$jjb\bar{b} + c.c$	$\epsilon_b^2 b_{jj}^W$	2	no	9.86×10^4	17.22
	0.16		yes	3.14×10^3	20.59
$pp \to W^+ZX + c.c.$					
$\ell^+\nu_\ell\ell'^+\ell'^- + c.c$	$b_{\ell\ell}^W b_{\ell\ell}^Z$	3	no	6.34×10^3	11.03
	0.0037		yes	1.08×10^2	3.63
$jj\ell^+\ell^- + c.c$	$b_{jj}^W b_{\ell\ell}^Z$	3	no	3.69×10^4	26.61
	0.0218		yes	6.26×10^2	8.75
$\ell^+\nu_\ell jj + c.c$	$b_{\ell\nu}^W b_{jj}^Z$	3	no	1.00×10^5	43.89
	0.0592		yes	1.70×10^3	14.43
$jjjj + c.c.$	$b_{jj}^W b_{jj}^Z$	3	no	5.84×10^5	105.84
	0.3443		yes	9.91×10^3	34.80
$jjb\bar{b} + c.c.$	$b_{jj}^W b_{bb}^Z \epsilon_b^2$	3	no	4.12×10^4	28.13
	0.0243		yes	7.00×10^2	9.25
$\ell^+\nu_\ell b\bar{b} + c.c.$	$b_{\ell\ell}^W b_{bb}^Z \epsilon_b^2$	3	no	7.12×10^3	11.69
	0.0042		yes	1.21×10^2	3.84
$pp \to W^+W^-X$					
$\ell_1^+\nu_{\ell_1}\ell_2^-\nu_{\ell_2}$	$(b_{\ell\ell}^W)^2$	3	no	3.86×10^4	12.73
	0.0121		yes	5.14×10^2	3.38
$\ell^+\nu_\ell jj$	$b_{\ell\ell}^W b_{jj}^W$	3	no	2.24×10^5	30.71
	0.0704		yes	2.99×10^3	8.16
$jjjj$	$(b_{jj}^W)^2$	3	no	1.30×10^6	74.07
	0.4096		yes	1.74×10^4	19.68

Table 4: Cross sections and statistical significance of the model signals for various decay channels of the analyzed processes. The integrated luminosity is $\mathcal{L} = 100$ fb^{-1}. The reduction factor r is the ratio between the cross sections of the process with the final state decayed and undecayed. The cut considered in Table is 0.7 TeV $\leq m_{34} \leq$ 1.1 TeV.

IV Conclusions

With the start of the LHC new era in attacking the question of the ESB mechanism begins. In this paper we have investigated the potential of the LHC processes $pp \to abX$, $ab = t\bar{t}, b\bar{b}, t\bar{b}, W^+Z, W^+W^-$, to probe a new vector $SU(2)_V$ triplet which might exist as a part of new physics responsible for ESB and, as far as fermions are concerned, it interacts directly to the third quark generation only. It is possible that new physics behind ESB can be effectively described by the HLS approach. Then the mixing of the vector resonances with the electroweak gauge bosons induces also interactions of ρ to lighter SM fermions.

The processes in which ρ interacts only to quarks of the third generation should be more sensitive to new physics than those which run through ρ-to-light-fermion vertices. However, at the LHC the former processes are often overwhelmed by a huge gluon-gluon background. We have seen this in the case of $pp \to t\bar{t}X$ and $pp \to b\bar{b}X$. We have demonstrated that also the processes where ρ couples to the light quarks in protons have a significant potential to distinguish our model from the light Higgs SM. We have calculated the statistical significance of the model signal for various decay channels of the final states. However, to decide whether and which of these channels can recognize the model at the LHC the further analysis, which would include the study of backgrounds and the detector reconstruction efficiency, is necessary. This is out of the scope of this paper, though. The results in this paper should help decide which of the processes are the best candidates for such further analyses.

References

[1] Cheng H-C, the proceedings of *15th International Conference on Supersymmetry and the Unification of Fundamental Interactions (SUSY07), Karlsruhe, Germany, 26 Jul - 1 Aug 2007*, hep-ph/0710.3407.

[2] Bando M, Kugo T, Yamawaki K, *Phys. Rep.* **164** (1988), 217.

[3] Coleman S R, Wess J, Zumino B, *Phys. Rev.* **177** (1969), 2239.

[4] Callan C G, Coleman S R, Wess J, Zumino B, *Phys. Rev.* **177** (1969), 2247.

[5] Casalbuoni R, et al., *Phys. Lett.* **B253** (1991), 275.

[6] Gintner M, Melo I, Trpišová B, *Acta Phys. Slov.* **56** (2006), 473-483.

[7] Boos E, et al. (CompHEP Collaboration), *Nucl. Instrum. Meth.* **A534** (2004), 250.

[8] Pukhov A, et al., hep-ph/9908288.